

# Northumbria Research Link

Citation: East, Holly, Perry, Chris T., Beetham, Eddie P., Kench, Paul S. and Liang, Yiqing (2020) Modelling reef hydrodynamics and sediment mobility under sea level rise in atoll reef island systems. *Global and Planetary Change*, 192. p. 103196. ISSN 0921-8181

Published by: Elsevier

URL: <https://doi.org/10.1016/j.gloplacha.2020.103196>  
<<https://doi.org/10.1016/j.gloplacha.2020.103196>>

This version was downloaded from Northumbria Research Link:  
<http://nrl.northumbria.ac.uk/id/eprint/43256/>

Northumbria University has developed Northumbria Research Link (NRL) to enable users to access the University's research output. Copyright © and moral rights for items on NRL are retained by the individual author(s) and/or other copyright owners. Single copies of full items can be reproduced, displayed or performed, and given to third parties in any format or medium for personal research or study, educational, or not-for-profit purposes without prior permission or charge, provided the authors, title and full bibliographic details are given, as well as a hyperlink and/or URL to the original metadata page. The content must not be changed in any way. Full items must not be sold commercially in any format or medium without formal permission of the copyright holder. The full policy is available online: <http://nrl.northumbria.ac.uk/policies.html>

This document may differ from the final, published version of the research and has been made available online in accordance with publisher policies. To read and/or cite from the published version of the research, please visit the publisher's website (a subscription may be required.)



# Modelling reef hydrodynamics and sediment mobility under sea level rise in atoll reef island systems



Holly K. East<sup>a,b,\*</sup>, Chris T. Perry<sup>b</sup>, Eddie P. Beetham<sup>c</sup>, Paul S. Kench<sup>c,d</sup>, Yiqing Liang<sup>c,e</sup>

<sup>a</sup> Department of Geography and Environmental Sciences, Faculty of Engineering and Environment, Northumbria University, Newcastle upon Tyne, UK

<sup>b</sup> Geography, College of Life and Environmental Sciences, University of Exeter, Exeter, UK

<sup>c</sup> School of Environment, University of Auckland, Auckland, New Zealand

<sup>d</sup> Department of Earth Sciences, Simon Fraser University, Burnaby, BC, Canada

<sup>e</sup> Department of Environmental Management, Faculty of Health, Humanities, and Computing, Southern Institute of Technology, Invercargill, New Zealand

## ARTICLE INFO

### Keywords:

Reef islands  
Sea level rise  
Waves  
Hydrodynamics  
Sediment transport  
Maldives

## ABSTRACT

Low-lying coral reef islands will be significantly impacted by future sea-level rise (SLR). It is generally expected that SLR will destabilise reef islands because increasing reef submergence allows larger waves, and therefore greater energy transmission, across reef flats. However, the potential impacts of SLR on reef flat sediment transport and sediment delivery to island shorelines are poorly understood. Here, we use the currents of removal approach (coupling two-dimensional wave modelling with settling velocity data from 186 benthic sediment samples) to model shifts in both reef hydrodynamics and benthic sediment transport under different scenarios of mean reef submergence (MRS = +0 m, +0.5 m, +1 m) at two atoll rim reef sites in the Maldives. Under contemporary conditions (MRS = +0 m), we found that benthic sediment transport is likely occurring, consistent with active reef-to-island sediment connectivity. Under conditions of increased MRS, shifts in wave velocities, and in turn sediment potential mobility, were both non-linear and non-uniform. Significant between-site differences were found in the magnitude of projected shifts in sediment mobility under scenarios of increased MRS, which implies that morphological responses to increased MRS are likely to be diverse, even over local scales. Under increased MRS, the largest increases in sediment mobility were projected on the inner reef flat, whereas lagoonal zones remained as sinks for sediment deposition. We thus hypothesize that while reef islands will persist as sedimentary landforms under projected rates of MRS, lagoonward reef island migration is likely to occur. Findings have implications for predicting the future adaptive capacity of atoll nations. Our results highlight the need for national-scale vulnerability assessments to incorporate (1) potential increases in island mobility; (2) the importance of allowing natural sediment transport processes to occur (unhindered by human constructions); and (3) intra-regional diversity in reef system geomorphic responses to sea level rise.

## 1. Introduction

Low-lying coral reef islands are frequently considered to be among the most vulnerable landforms to climate change and associated sea-level rise (SLR; IPCC et al., 2019). Increases in flooding and wave inundation events have been projected to render atoll nations uninhabitable by the end of the century (Quataert et al., 2015; Storlazzi et al., 2015, 2018). Given their vulnerability, reef islands have received increasing attention from geomorphic (Webb and Kench, 2010; Kench et al., 2015; Duvat et al., 2017; Kench et al., 2018) and hydrodynamic

(Quataert et al., 2015; Storlazzi et al., 2015, 2018; Beetham et al., 2017) research in recent years. However, existing research efforts have largely focussed on individual elements of the reef system without accounting for the important morphodynamic interactions that operate within reef systems. One significant limitation of prior work is that sediment transport processes remain poorly constrained. This knowledge gap is particularly pertinent given that reef islands are formed entirely of sediments produced by organisms in their adjacent marine environments. Sediment transport processes are thus key controls on reef island maintenance and morphological stability. Despite their

*Abbreviation:* MRS, mean reef submergence; SLR, sea level rise; PM, potential mobility;  $V_{mean}$ , mean wave-induced velocities;  $V_{max}$ , maximum wave-induced velocities

\* Corresponding author at: Department of Geography and Environmental Sciences, Faculty of Engineering and Environment, Northumbria University, Newcastle upon Tyne, UK.

E-mail address: [holly.east@northumbria.ac.uk](mailto:holly.east@northumbria.ac.uk) (H.K. East).

<https://doi.org/10.1016/j.gloplacha.2020.103196>

Received 1 November 2019; Received in revised form 27 March 2020; Accepted 18 April 2020

Available online 01 May 2020

0921-8181/© 2020 The Authors. Published by Elsevier B.V. This is an open access article under the CC BY license

(<http://creativecommons.org/licenses/by/4.0/>).

importance, there is very limited understanding of both contemporary process regimes and how these processes may change under future SLR scenarios.

One reason for the paucity of prior research on reefal sediment transport processes is that the classic empirical expressions of clastic sediment entrainment, transport and deposition (Hjulstrom, 1935; Shields, 1936; Rouse, 1937) are of limited value in reef environments (Scoffin, 1992; Cuttler et al., 2017). The biogenic nature of reefal sediment, which is derived from a variety of source organisms (e.g. coral, molluscs, foraminifera), results in grains of variable density, size and shape (Sorby, 1879; Chave et al., 1972; Ford and Kench, 2012). Reefal sediments thus violate the assumptions of traditional sediment transport expressions that employ grain size as the primary control on clastic sediment entrainment (Maiklem, 1968; Braithwaite, 1973; Kench and McLean, 1996). To address these challenges, the ‘currents of removal’ approach was developed to provide a more robust means of quantifying reefal sediment transport by analysing sediment hydrodynamic properties (as opposed to grain size) in combination with hydrodynamic data (Scoffin, 1987; Kench, 1998). Despite the development of the ‘currents of removal’ approach, there has been limited application of such approaches to better understand sediment hydrodynamics and transport processes in reef systems. Whilst there is a growing body of literature examining sediment transport processes under modal conditions (e.g. Morgan and Kench, 2016; Pomeroy et al., 2018; Cuttler et al., 2019), there remains a paucity of research into sediment transport dynamics under SLR. A notable exception is work on transport dynamics under SLR scenarios on fringing type reef systems in Hawaii, using numerical modelling in one-dimension (Ogston and Field, 2010) and of profiles in two-dimensions (Storlazzi et al., 2011; Grady et al., 2013). To the best of our knowledge, the only work to investigate sediment transport under SLR in atoll reef island environments has been analyses of shifts in alongshore sediment transport (Shope et al., 2017; Shope and Storlazzi, 2019). We thus present the first analysis of reef island sediment transport under SLR across atoll reef island platforms. Understanding of these processes is especially limited in low-lying atoll reef island systems, yet this knowledge is critical to better constrain future reef island landform trajectories and, in turn, to inform national-scale vulnerability assessments of reef island nations.

Here, we use the ‘currents of removal’ approach to present the first study of both hydrodynamics and benthic sediment transport under different mean reef submergence (MRS) scenarios across atoll reef island platforms. We refer to MRS, as opposed to SLR, as to solely consider SLR assumes that reef morphology remains static (i.e. no reef growth will occur over the associated timeframe). Rather, we suggest it is more appropriate to employ MRS as it is the difference between vertical reef accretion and SLR that is the key control on across-reef wave energy regimes (Quataert et al., 2015). Data are presented from two contrasting settings (in terms of exposure to open ocean swell) on Huvadho atoll rim, southern Maldives. We use two-dimensional modelling to simulate wave processes under three scenarios: MRS = +0 m (contemporary conditions), +0.5 m (SLR and reef accretion data from the southern Maldives suggest this would occur by 2100 under RCP8.5; Perry et al., 2018), and +1 m (projected as the upper extreme in the southern Maldives by 2100 under RCP8.5, 95% confidence interval; Perry et al., 2018). Wave model outputs are then coupled with settling velocity data from 186 benthic sediment samples to estimate sediment potential mobility (PM) under each of these MRS scenarios. Results are discussed in the context of the geomorphic implications for reef island futures. We suggest that while reef islands may persist under SLR, there will likely be increased island mobility and local-scale variability in the magnitude of such morphological shifts.

## 2. Regional setting

The Maldives is a reef island nation comprised of ~1,200 islands inhabited by a population of ~436,000 (Fig. 1). There is an emerging

understanding of reef hydrodynamics (Kench et al., 2006; Mandrier, 2008) and sediment transport (Morgan and Kench, 2014, 2016) under the contemporary process regime on faro type reef platforms (i.e. small annular atoll interior reef platforms) in the Maldives. However, our understanding of reef hydrodynamics and sediment transport on Maldivian linear atoll rim platforms (i.e. elongate reef platforms which form atoll perimeters) is limited. This is a key knowledge gap as sediment transport processes are likely to differ significantly between faro and linear rim platforms as they have distinctly different process regimes. Linear rim platforms are characterised by strong cross-platform wave energy gradients, whereas waves converge at a focal point on faro surfaces as wave energy is incident around 360° of their platform margins (Kench, 2013).

Straddling the equator, the Maldives archipelago is located in a predominantly storm-free environment (Woodroffe, 1993; Fig. 1). Satellite altimetry data indicate that oceanic swell approaches from southeasterly directions between November and March, and south to south-westerly directions between April and November (Young, 1999). Our study focused on Huvadho Atoll, which is approximately 60 km in width, 80 km in length and has an area of 3279 km<sup>2</sup> (Naseer and Hatcher, 2004). Two sections of Huvadho Atoll rim were selected as study sites, which represent end-members with respect to their relative exposure to open oceanic swell: a north-eastern leeward site (which contains Galamadho island), and a south-western windward site (which contains Mainadho, Boduhini and Kudahini islands). The areal extents of the marine environments in the windward and leeward sites are 0.84 km<sup>2</sup> and 1.06 km<sup>2</sup>, respectively (Table A1). To characterise the oceanic process regime, wave parameters were extracted from Wave-Watch III model hindcasts (Tolman, 2009; Durrant et al., 2013) for the period 1979 to 2010 at locations 20 km off the oceanward platform margin at each site. The significant wave height and significant wave period were found to be significantly higher and longer at the windward than the leeward site respectively (paired *t*-tests; *P* ≤ .001; East et al., 2018).

## 3. Materials and methods

### 3.1. Eco-geomorphic zonation

As a means of structuring sampling design, eco-geomorphic zones were identified at each site (Table A1). Zones were selected based on preliminary field surveys and examination of satellite imagery to characterise the range of substrate types, hydrodynamic settings and ecological communities (Perry et al., 2015). High resolution satellite imagery was used to generate digital habitat maps of the eco-geomorphic zones at each site (Fig. 1). A WorldView-2 image of the leeward site was acquired on 13th April 2015, and a Quickbird image of the windward site was acquired on 27th May 2010 (spatial resolution of visible optical bands = 1.86 m and 2.40 m, respectively). Both images were cloud- and sun glint-free. A Maximum Likelihood Classification was performed on the atmospherically corrected bands. Ground truth data were obtained from each zone (04–06/2013; *n* = 190 and *n* = 210 for the leeward and windward sites, respectively), which were divided to train (20%) and validate (80%) the classifications. Overall classification accuracies (the number of correctly identified pixels divided by the total number of pixels in the validation; Congalton, 1991) were 88.0% and 91.1% at the windward and leeward sites, respectively.

### 3.2. Hydrodynamic processes

To simulate wave processes, two-dimensional depth-averaged wave modelling was undertaken using a Green-Naghdi (GN) free-surface solver from the open source model Basilisk (Popinet, 2015). This approach has been demonstrated to be effective in simulating wave dispersion, wave breaking, and wet-dry interaction in shallow coastal environments (Bonneton et al., 2011; Tissier et al., 2012; Lannes and

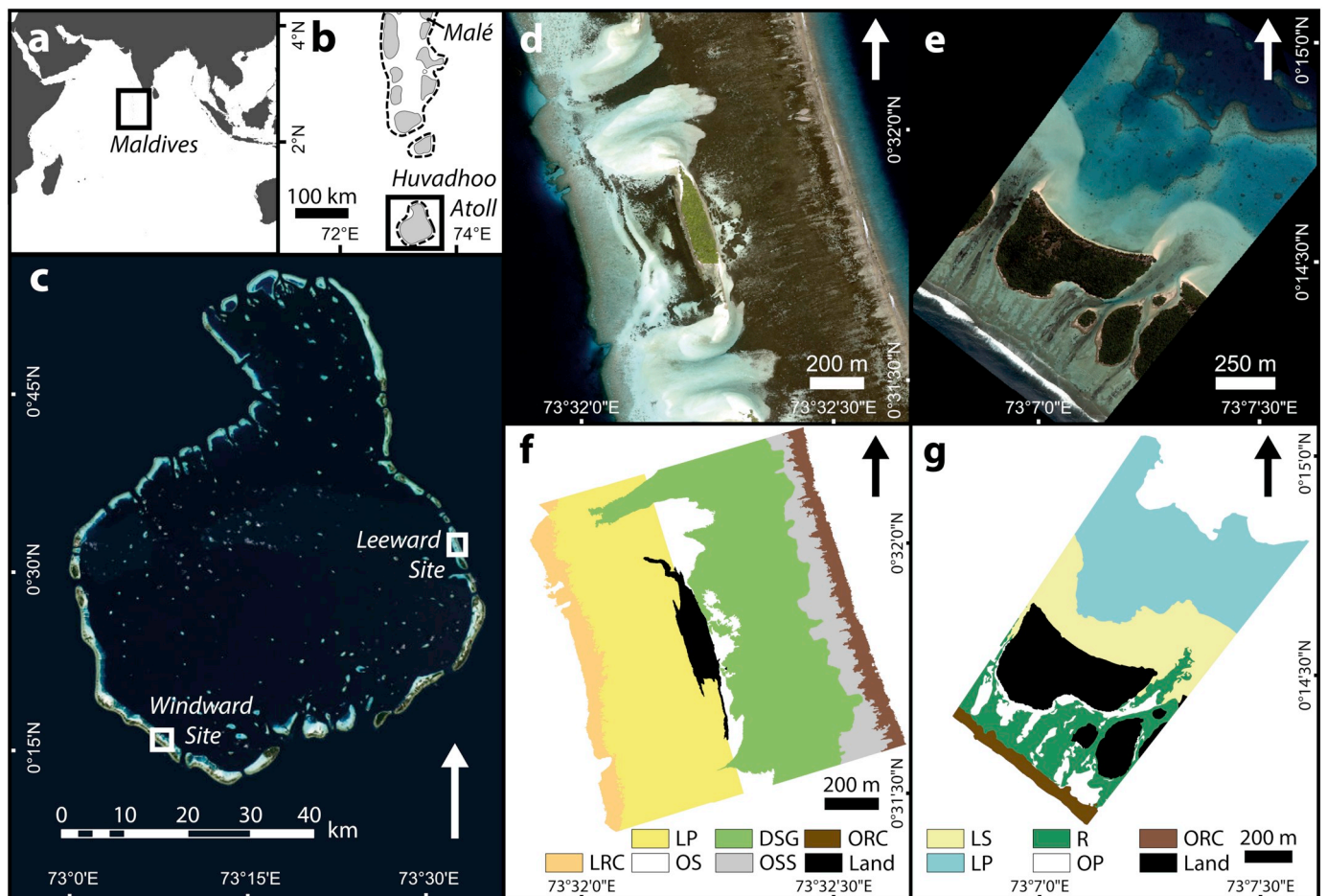


**Fig. 1.** Location of the Maldives (a), Huvadho Atoll (b), and leeward and windward study sites (c). Satellite imagery and classifications of eco-geomorphic zones at the leeward (d, f) and windward (e, g) sites. At the leeward site, LRC = lagoonward reef crest, LP = lagoonward patch (reef), OS = oceanward sand, DSG = dense seagrass, OSS = oceanward sparser seagrass, and ORC = oceanward reef crest. At the windward site, LP = lagoonward patch (reef), LS = lagoonward sand, OP = oceanward patch (reef), R = rubble, and ORC = oceanward reef crest.

Marche, 2015). Basilisk GN is able to simulate the behaviour of relatively large amplitude waves across a sudden change in bathymetry (i.e. across a reef crest), which is a challenge for traditional Boussinesq-type models (Roeber and Cheung, 2012). The Basilisk GN solver has also been comprehensively evaluated for accurately simulating surf-zone processes in complex reef settings. Benchmark model testing for 1D and 2D scenarios of wave iteration with reefs produced high skill for resolving free surface and velocity across the domain (Beetham et al., 2018). The model has also been proven to successfully replicate field measurements of wave transformation, infragravity wave propagation and wave setup when compared to measurements from an atoll reef in Tuvalu (Beetham et al., 2016). A significant capability of the phase-resolving model is that both currents driven by the orbital motions of individual waves and the mean currents driven by wave setup gradients are represented. The grid size was uniform across the domain with a  $5 \times 5$  m cell size. A consistent implicit quadratic bottom friction coefficient of 0.04 was applied across the model domain. This value was obtained from previous tests of different friction scenarios for implicit quadratic bottom friction across a similar atoll rim reef in Tuvalu, which was comprised of coral, coralline algae, rubble and pavement (Beetham et al., 2016).

Bathymetric data were required as inputs to the wave model. Bathymetric digital elevation models of the windward and leeward sites were derived from Quickbird and WorldView-2 imagery, respectively. Water depths were obtained in the field using a single beam echosounder to obtain 400 individual soundings ( $n = 210$  and  $n = 190$  at

the windward and leeward sites, respectively), which were corrected relative to MSL using the tide tables for Gan ( $00^{\circ}41'S$ ,  $73^{\circ}9'E$ ) from the University of Hawaii Sea Level Centre (depth range = 0 to 17 m below MSL). UK Hydrographic Office (1992) charts were used to supplement field data with depths from beyond the oceanward platform margin (these areas were inaccessible due to large oceanic waves; depth range = 15 to 55 m below MSL). Field datasets were then divided to calibrate (50%) and validate (50%) the bathymetric models. Models were generated following the methodology of Stumpf et al. (2003), which applies a band ratio transformation whereby the green and blue bands were extracted from atmospherically corrected images. A ratio layer was produced by dividing the natural log of the green band by the natural log of the blue band. Ratio values were plotted against the calibration data and a second-order polynomial relationship was fitted. The regression equations were applied to the ratio layers to estimate bathymetry across the entirety of each site (spatial resolution = 2.4 m and 1.86 m at the windward and leeward sites, respectively). To validate the models, the field-derived depths of the validation dataset were compared to the model-derived depths (Hamylton et al., 2015). The correlation between field- and model-derived depths was strongly positive in both cases ( $R^2 = 0.86$  and  $0.83$  at the windward and leeward sites, respectively; Table A1).

Wave height and period data at the lagoonward and oceanward margins of the reef platforms were also required as inputs to the wave model (Table 1). Wave climate data were acquired from three sources. Firstly, oceanward wave data were extracted from WaveWatch III

**Table 1**

Wave data employed as model inputs from the oceanward and lagoonward margins for both the windward and leeward study sites.

Model inputs		Windward site	Leeward site	Data source
Oceanward margin	$H_s$ (m)	1.55	1.35	WaveWatch III
	$T_s$ (s)	10.1	8.8	WaveWatch III
Lagoonward margin	$H_s$ (m)	0.12 <sup>a</sup>	0.6 <sup>b</sup>	<sup>a</sup> Field data
	$T_s$ (s)	8.5 <sup>a</sup>	4 <sup>b</sup>	<sup>b</sup> Linear wave theory

$H_s$  = significant wave height (m),  $T_s$  = significant wave period (s).

model hindcasts (Tolman, 2009; Durrant et al., 2013) for the period 1979 to 2010 at locations 20 km off the oceanward platform margin at each site. Significant wave height and period were extracted and the average taken in order to investigate fair-weather conditions. Secondly, lagoonward wave data for the windward site were obtained from an 8-day field experiment between 8th and 16th November 2007 over 16 successive high tidal stages (Mandlier, 2008). Also with the aim of examining a windward rim setting, Mandlier placed instruments at Fares-Maathodaa. Fares-Maathodaa is located ~8 km to the east of the windward site and the platform has a similar aspect relative to incident swell, providing confidence that lagoonward wave conditions are comparable. Mandlier (2008) also collected wave data in the centre of the windward reef platform in a location that approximately corresponds with the lagoonward sand zone in this study. Notably, root mean square wave height ( $H_{rms}$ ; average  $H_{rms}$  = ~0.05 m) was found to be comparable to that suggested by the model outputs in the present study (average  $H_{rms}$  = 0.03 ± 0.05 m; Table A2). Thirdly, lagoonward data for the leeward site were calculated using linear wave theory through application of the JONSWAP approach (Hasselmann et al., 1973) with the revisions suggested by the Shore Protection Manual (1984). Calculations were undertaken using the SwellBeat (2020) Wave Calculator with (1) windspeeds of 10 knots, the average prevailing westerly windspeed calculated using 2014 wind data ( $n$  = 2643) from Kaadedhdhoo Airport (0.49°N, 73.00°E; Wunderground, 2015); (2) a duration of 24 h; and (3) a fetch length of 55 km (westerly distance across the atoll lagoon). In each case, an irregular wave field was imported into both the lagoonward and oceanward fields. The model ran for 2048 s with a spatial resolution of 5.8 m.

The model was run three times for each site using different scenarios of mean reef submergence (MRS): +0 m (i.e. contemporary conditions), +0.5 m and +1 m. Mean ( $V_{mean}$ ) and maximum ( $V_{max}$ ) wave-induced velocities were extracted from the model outputs. The mean velocity ( $V_{mean}$ ) was calculated for each cell as the average velocity value between  $t$  = 400 s and 2048 s (i.e. the period during which the wave field was fully developed) and is representative of average currents due to spatial variability in wave setup.  $V_{max}$  is the maximum value within each cell between  $t$  = 400 s and 2048 s and represents wave-driven (short-period) velocities. Hence, both  $V_{mean}$  and  $V_{max}$  occur under fair-weather conditions with a fully developed wave field. Use of  $V_{mean}$  and  $V_{max}$  is consistent with the development and prior applications of the currents of removal approach (Kench, 1998). To compare  $V_{max}$  with upper wave velocity results, V2% was calculated. A comparative analysis of  $V_{max}$  and V2% was undertaken and the results were found to be similar (Fig. A1). Root mean square wave height ( $H_{rms}$ ) and setup (mean displacement of the free surface; i.e. the difference between absolute depth and time-averaged water level) were also calculated for each cell in the model domain to assess differences in wave transformation between scenarios (Table A2; Fig. A2–A5).

### 3.3. Sediment transport

A total of 186 benthic surficial sediment samples were collected: 90 from the windward site and 96 from the leeward site (Fig. A6). Equal numbers of samples were collected from each eco-geomorphic zone

( $n$  = 15 and  $n$  = 16 from each zone at the windward and leeward sites, respectively). Each sediment sample was hand scooped using a 500 ml sample pot, rinsed in freshwater twice for 12 h, soaked in a 5% bleach solution for 24 h (to neutralise organic matter), and oven dried (40 °C). Sediment was relatively homogeneous in character, comprised of predominantly coral (72.1 ± 0.5%), with lesser proportions of CCA (11.5 ± 0.4%) and molluscs (9.1 ± 0.4%; East, 2017). The hydraulic characteristics of sand-sized (0.063 mm – 2 mm; –1–4  $\phi$ ) sediment were measured by settling a 15 g sub-sample (obtained using a riffle splitter) through a McArthur Rapid Sediment Analyser (RSA) with a vertical fall of 1.75 m. A time-series of weight accumulation on the balance plate was recorded to calculate the settling velocity distribution ( $\chi$ ) and the mean settling velocity ( $\text{cm s}^{-1}$ ; Table A3). Sediment grain size distributions were calculated using the equations of Gibbs et al. (1971) with a grain density of 1.85 g  $\text{cm}^3$ .

The ‘currents of removal’ approach was used to calculate the Potential Mobility (PM) of each sediment sample following the methodology proposed and validated by Kench (1998). PM is defined as the proportion (%) of a sample that can be mobilised under normal (i.e. ‘fair-weather’) conditions and is calculated using wave velocity data in combination with the sediment settling velocity distributions ( $\chi$ ). Firstly, wave velocities at each sediment sample location were extracted from wave process model outputs and were used to calculate the mean threshold settling velocity ( $\chi$ ) for each sediment sample using the experimentally-derived entrainment threshold relationship for bioclastic sediments reported by Kench and McLean (1996,  $R^2$  = 0.93). Secondly, the settling velocity threshold ( $\chi$ ) at each sample location was calculated on each settling velocity curve of the concerned sediment sample. PM is the proportion of the sample with equal or slower settling velocity than the threshold value. This approach was applied six times at each study site: for mean ( $V_{mean}$ ) and maximum ( $V_{max}$ ) velocities associated with MRS = +0 m, +0.5 m and +1 m. In order to visualise spatial variability, results were interpolated using a block kriging algorithm, whereby kriging was undertaken within, but not across the boundaries of, each eco-geomorphic zone (spatial resolution = 6 m).

## 4. Results

### 4.1. Contemporary process regime

At both sites,  $V_{mean}$  was at a maximum off the oceanward rim, before waves reached the oceanward reef crest zone (~1.18 m  $\text{s}^{-1}$  and ~0.70 m  $\text{s}^{-1}$  at the windward and leeward sites respectively; Fig. 2, A7–A10; Table 2), and rapidly decreased within the oceanward reef crest zones (0.39 ± 0.02 m  $\text{s}^{-1}$  and 0.08 ± 0.01 m  $\text{s}^{-1}$  at the windward and leeward sites, respectively; Table 2). There was an oceanward-lagoonward decay in  $V_{mean}$  with minimum values found off lagoonward island shorelines (0.01 m  $\text{s}^{-1}$ ). Converse to the oceanward-lagoonward gradient, increases in  $V_{mean}$  were found within inter-island passages, particularly at the windward site (up to 0.75 m  $\text{s}^{-1}$ ). At the leeward site, there was a slight increase in  $V_{mean}$  toward the lagoonward platform margin ( $V_{mean}$  = 0.07 ± 0.03 m  $\text{s}^{-1}$  in the lagoonward reef crest zone). Under  $V_{max}$ , trends were comparable though velocities were higher with proximity to the oceanward platform margin whereby  $V_{max}$  = 1.36 ± 0.28 m  $\text{s}^{-1}$  and 0.94 ± 0.26 m  $\text{s}^{-1}$  within the oceanward reef crest zones at the windward and leeward sites, respectively (Fig. 2, A7–A10; Table 2).

As a function of spatial trends in wave velocities, PM data indicated that the predominant direction of sediment transport was along gradients from high PM at the oceanward reef crest to low PM at the lagoonward platform margin (Figs. 3, 4, A11–A16; Table 3). At the windward site, under  $V_{mean}$  benthic sediment transport occurred from the oceanward reef crest (20.4 ± 13.7%) into the remainder of the oceanward environment (PM = ~10%), through inter-island passages (up to 100%), and into the lagoonward environment where sediment

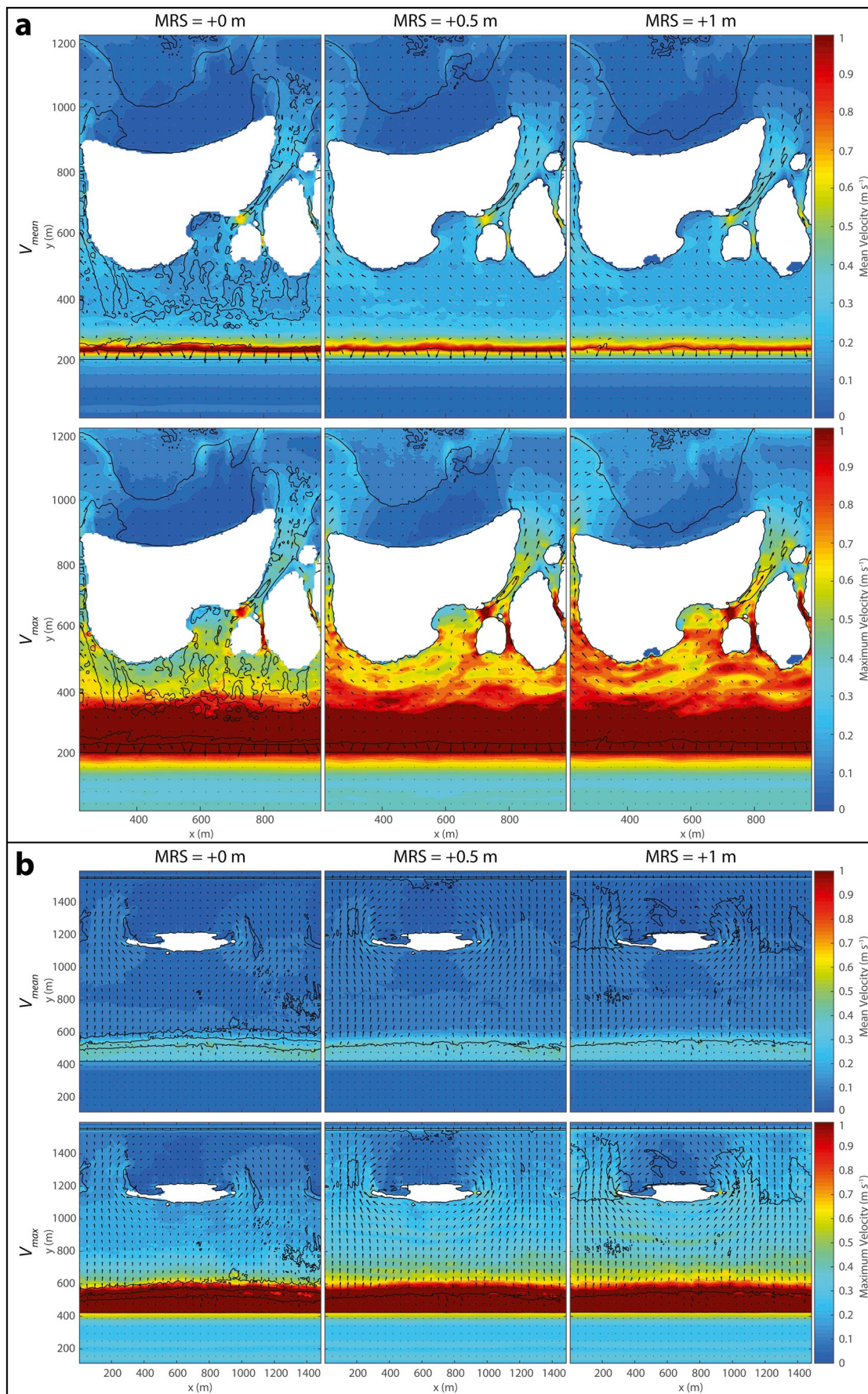


**Fig. 2.** Mean ( $V_{mean}$ ) and maximum ( $V_{max}$ ) velocities ( $m s^{-1}$ ) across the windward (a) and leeward (b) sites where MRS = +0 m, +0.5 m, and +1 m. Vectors represent the direction and magnitude of the velocity plotted in each panel.

**Table 2**

Mean ( $V_{mean}$ ) and maximum ( $V_{max}$ ) wave velocities ( $m s^{-1}$ , mean  $\pm$  1 S.D., ranges in italics) within each eco-geomorphic zone where MRS = +0 m, +0.5 m and +1 m.

Site	Zone	MRS = +0 m		MRS = +0.5 m		MRS = +1 m		
		Mean $\pm$ 1 S.D.	Range	Mean $\pm$ 1 S.D.	Range	Mean $\pm$ 1 S.D.	Range	
Windward	$V_{mean}$ ( $m s^{-1}$ )	ORC	0.28 $\pm$ 0.05	<i>0.17–0.52</i>	0.29 $\pm$ 0.05	<i>0.21–0.53</i>	0.31 $\pm$ 0.05	<i>0.22–0.56</i>
		R	0.22 $\pm$ 0.08	<i>0–0.78</i>	0.25 $\pm$ 0.08	<i>0–0.77</i>	0.24 $\pm$ 0.07	<i>0–0.71</i>
		OP	0.19 $\pm$ 0.09	<i>0–0.61</i>	0.21 $\pm$ 0.1	<i>0–0.72</i>	0.22 $\pm$ 0.09	<i>0–0.67</i>
		LS	0.1 $\pm$ 0.07	<i>0–0.54</i>	0.11 $\pm$ 0.08	<i>0–0.45</i>	0.11 $\pm$ 0.08	<i>0–0.49</i>
		LP	0.08 $\pm$ 0.03	<i>0.03–0.2</i>	0.08 $\pm$ 0.03	<i>0.04–0.19</i>	0.08 $\pm$ 0.02	<i>0.04–0.18</i>
	$V_{max}$ ( $m s^{-1}$ )	ORC	1.36 $\pm$ 0.28	<i>0.7–2.55</i>	1.33 $\pm$ 0.25	<i>0.85–2.29</i>	1.24 $\pm$ 0.22	<i>0.81–2.17</i>
		R	0.52 $\pm$ 0.22	<i>0–1.37</i>	0.64 $\pm$ 0.23	<i>0–1.57</i>	0.7 $\pm$ 0.22	<i>0–1.51</i>
		OP	0.51 $\pm$ 0.25	<i>0–1.22</i>	0.63 $\pm$ 0.28	<i>0–1.26</i>	0.67 $\pm$ 0.27	<i>0–1.25</i>
		LS	0.14 $\pm$ 0.11	<i>0–0.71</i>	0.18 $\pm$ 0.12	<i>0–0.68</i>	0.22 $\pm$ 0.13	<i>0–0.77</i>
		LP	0.14 $\pm$ 0.05	<i>0.04–0.36</i>	0.15 $\pm$ 0.04	<i>0.08–0.32</i>	0.17 $\pm$ 0.04	<i>0.1–0.35</i>
Leeward	$V_{mean}$ ( $m s^{-1}$ )	ORC	0.22 $\pm$ 0.07	<i>0.11–0.47</i>	0.23 $\pm$ 0.07	<i>0.12–0.46</i>	0.25 $\pm$ 0.07	<i>0.13–0.44</i>
		OSS	0.12 $\pm$ 0.01	<i>0.06–0.21</i>	0.12 $\pm$ 0.01	<i>0.1–0.23</i>	0.13 $\pm$ 0.02	<i>0.11–0.26</i>
		DSG	0.1 $\pm$ 0.02	<i>0–0.45</i>	0.11 $\pm$ 0.01	<i>0.04–0.34</i>	0.11 $\pm$ 0.01	<i>0.05–0.19</i>
		OS	0.11 $\pm$ 0.03	<i>0–0.31</i>	0.12 $\pm$ 0.03	<i>0–0.29</i>	0.12 $\pm$ 0.03	<i>0–0.25</i>
		LP	0.06 $\pm$ 0.04	<i>0–0.33</i>	0.08 $\pm$ 0.04	<i>0–0.43</i>	0.07 $\pm$ 0.03	<i>0–0.29</i>
	$V_{max}$ ( $m s^{-1}$ )	LRC	0.07 $\pm$ 0.03	<i>0.02–0.16</i>	0.07 $\pm$ 0.03	<i>0.04–0.16</i>	0.08 $\pm$ 0.03	<i>0.04–0.15</i>
		ORC	0.94 $\pm$ 0.26	<i>0.45–1.66</i>	0.96 $\pm$ 0.21	<i>0.54–1.6</i>	0.94 $\pm$ 0.17	<i>0.57–1.49</i>
		OSS	0.46 $\pm$ 0.09	<i>0.22–0.97</i>	0.55 $\pm$ 0.08	<i>0.38–1</i>	0.58 $\pm$ 0.08	<i>0.42–0.96</i>
		DSG	0.24 $\pm$ 0.06	<i>0–0.54</i>	0.34 $\pm$ 0.07	<i>0.13–0.58</i>	0.38 $\pm$ 0.06	<i>0.18–0.61</i>
		OS	0.2 $\pm$ 0.04	<i>0–0.4</i>	0.29 $\pm$ 0.05	<i>0–0.59</i>	0.34 $\pm$ 0.05	<i>0–0.62</i>
	LP	0.1 $\pm$ 0.06	<i>0–0.4</i>	0.15 $\pm$ 0.07	<i>0–0.62</i>	0.18 $\pm$ 0.08	<i>0–0.66</i>	
	LRC	0.13 $\pm$ 0.07	<i>0.05–0.33</i>	0.15 $\pm$ 0.08	<i>0.06–0.39</i>	0.16 $\pm$ 0.09	<i>0.07–0.42</i>	

At the windward site, LP = lagoonward patch, LS = lagoonward sand, OP = oceanward patch, R = rubble, and ORC = oceanward reef crest. At the leeward site, LRC = lagoonward reef crest, LP = lagoonward patch, OS = oceanward sand, DSG = dense seagrass, OSS = oceanward sparser seagrass, and ORC = oceanward reef crest.

transport occurred in the lee of the inter-island passages (up to 24%). Under  $V_{max}$ , there was greater potential for sediment mobility. Sediment was transported from the oceanward environment (PM = ~100%), through inter-island passages (PM = ~100%), and into the lagoonward sand zone (PM =  $8.3 \pm 24.7\%$ ). The lagoonward sand zone remained predominantly immobile, except in the lee of the inter-island passages (PM = up to 99%).

At the leeward site, PM was lower than that at the windward site. Under  $V_{mean}$ , the only potentially mobilised sediment was found within the reef crest zones (average PM = up to 2%). Under  $V_{max}$ , PM remained low within the lagoonward zones (average PM = up to 3%), but there was a marked increase in PM of oceanward sediments. Oceanward-lagoonward sediment transport thus likely occurred with progressively decreasing proportions of mobile material from the oceanward reef crest zone (PM = 100%), through the oceanward sparser seagrass (PM =  $97.3 \pm 8.2\%$ ) and dense seagrass (PM =  $38.3 \pm 26.3\%$ ) zones, and towards the oceanward sand zone (PM =  $7.7 \pm 7.8\%$ ).

Differences were found in the grain size of potentially mobilised sediment between eco-geomorphic zones (Figs. A15, A16). At the windward site under  $V_{mean}$ , material able to be mobilised had a grain size of up to medium-coarse grained sand ( $> \sim 1 \phi$ ) in the oceanward reef crest zone, and up to medium-grained sand ( $> \sim 1-2 \phi$ ) across the remainder of the oceanward environment. Within the lagoonward zones, only silt-sized sediment could be mobilised ( $> 4 \phi$ ). Under  $V_{max}$ , very coarse sand could be mobilised across the oceanward zones ( $> -1 \phi$ ). In the lagoonward environment, fine to very fine sand ( $> \sim 3 \phi$ ) and fine grade sand ( $> \sim 2.5 \phi$ ) could be potentially mobilised in the lagoonward sand and patch zones, respectively. At the leeward site under  $V_{mean}$ , only fine sand ( $> \sim 2.5 \phi$ ) was potentially mobile. Under  $V_{max}$ , very coarse sand ( $> \sim -0.7 \phi$ ) could be mobilised on the oceanward reef crest. There was an oceanward-lagoonward decrease in the grain size of potentially mobilised material to medium-fine sand ( $> \sim 2 \phi$ ) in the oceanward sand zone. Within the lagoonward environment, only fine-grained material ( $> \sim 1.8 \phi$ ) could be mobilised.

#### 4.2. Future process regimes

Under scenarios of increased MRS, shifts in wave velocities were both non-linear and non-uniform (Table 2; Fig. 2, A7-A10). Relatively marginal increases in  $V_{mean}$  were projected at both sites (Fig. 2) with average increases of up to  $0.03 m s^{-1}$ . However, shifts in  $V_{max}$  under increased MRS scenarios were projected to be more pronounced than those associated with  $V_{mean}$ , though also non-linear and non-uniform (Fig. 2). In the oceanward reef crest zone at the windward site,  $V_{max}$  decreased by  $0.03 m s^{-1}$  between +0 and +0.5 m MRS, and by a further  $0.09 m s^{-1}$  between +0.5 and +1 m MRS. In the leeward site oceanward reef crest zone, shifts in  $V_{max}$  were only marginal ( $\sim 0.02 m s^{-1}$ ). In contrast, marked increases in  $V_{max}$  were found across the remainder of the oceanward environment. For example,  $V_{max}$  was projected to increase by  $\sim 0.18 m s^{-1}$  in the windward site rubble zone. Similarly, at the leeward site,  $V_{max}$  increased by  $\sim 0.14 m s^{-1}$  between +0 and +1 m MRS scenarios in the oceanward sand and dense seagrass zones. In the lagoonward environments, increases in  $V_{max}$  were projected to be smaller in magnitude (average increases of up to  $\sim 0.08 m s^{-1}$  between +0 and +1 m MRS).

Sediment PM was projected to increase under scenarios of increased MRS (Table 3; Figs. 3, 4, A11, A12). At the windward site under  $V_{mean}$ , PM was projected to increase across the oceanward zones, though in a non-linear manner. For example, increases in PM were of greater magnitude between +0 and +0.5 m MRS (by ~9% and ~5% within the rubble and oceanward patch zones) than between +0.5 and +1 m MRS (by ~1% and ~0.5%). Projected increases in PM at the windward site under  $V_{mean}$  were significant between both MRS increments (+0 to +0.5 m and +0.5 to +1 m,  $P \leq .0005$ , Wilcoxon signed ranks tests). Under  $V_{max}$ , sediment across the entirety of the windward site oceanward environment attained 100% PM under both scenarios of increased MRS. Converse to PM under  $V_{mean}$ , PM in the lagoonward patch zone ( $22.4 \pm 26.4\%$  and  $30.6 \pm 33.8\%$ ) was projected to exceed that in the lagoonward sand zone ( $15.0 \pm 29.5\%$  and  $22.7 \pm 38.6\%$ ). However, variability remained high due to high PM values within the lee of the inter-island passages (up to 100%). Under  $V_{max}$  at the

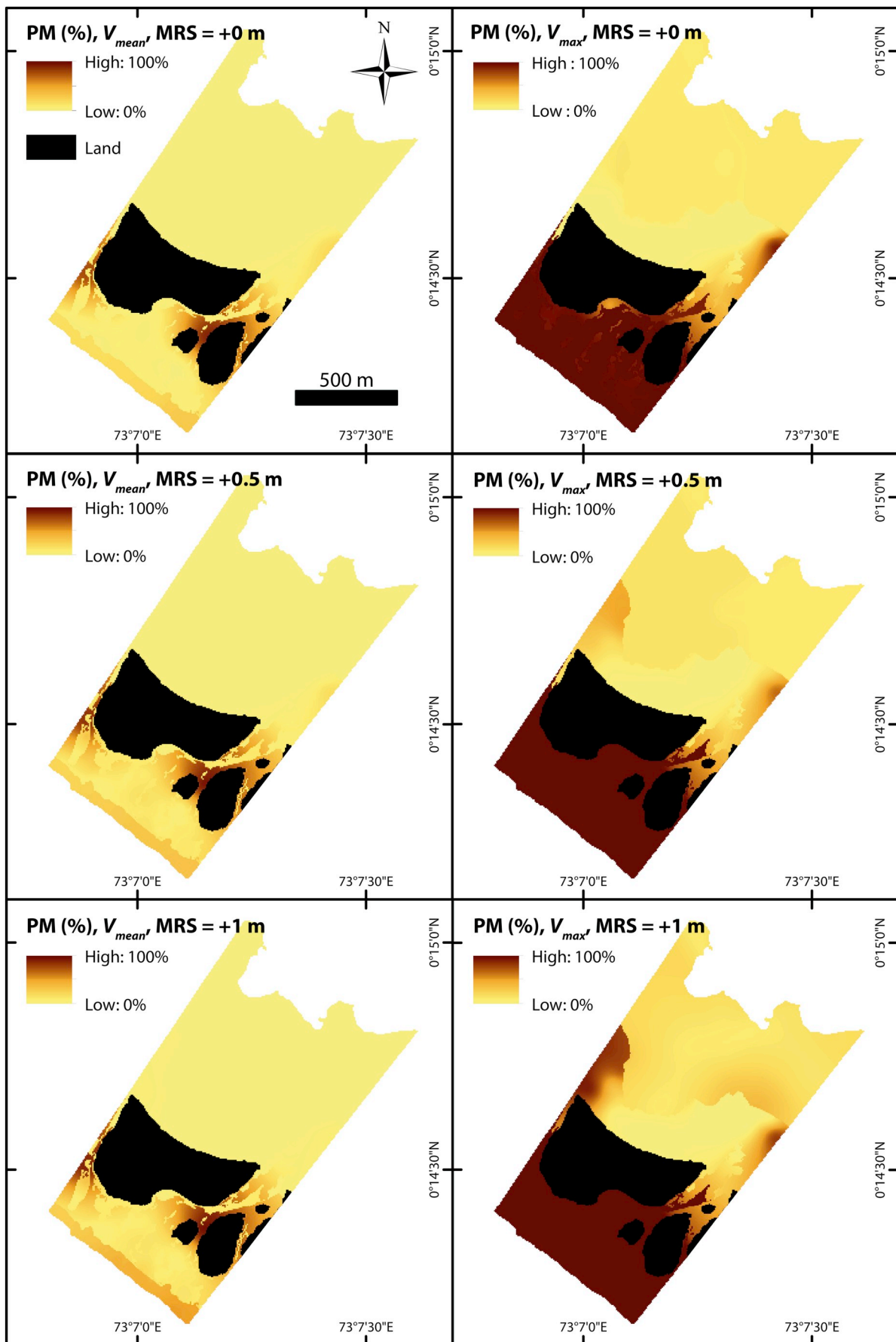


Fig. 3. Windward site block kriging results of sediment potential mobility (PM, %) with both mean ( $V_{mean}$ ) and maximum ( $V_{max}$ ) velocities under scenarios of +0 m, +0.5 m, and +1 m MRS.



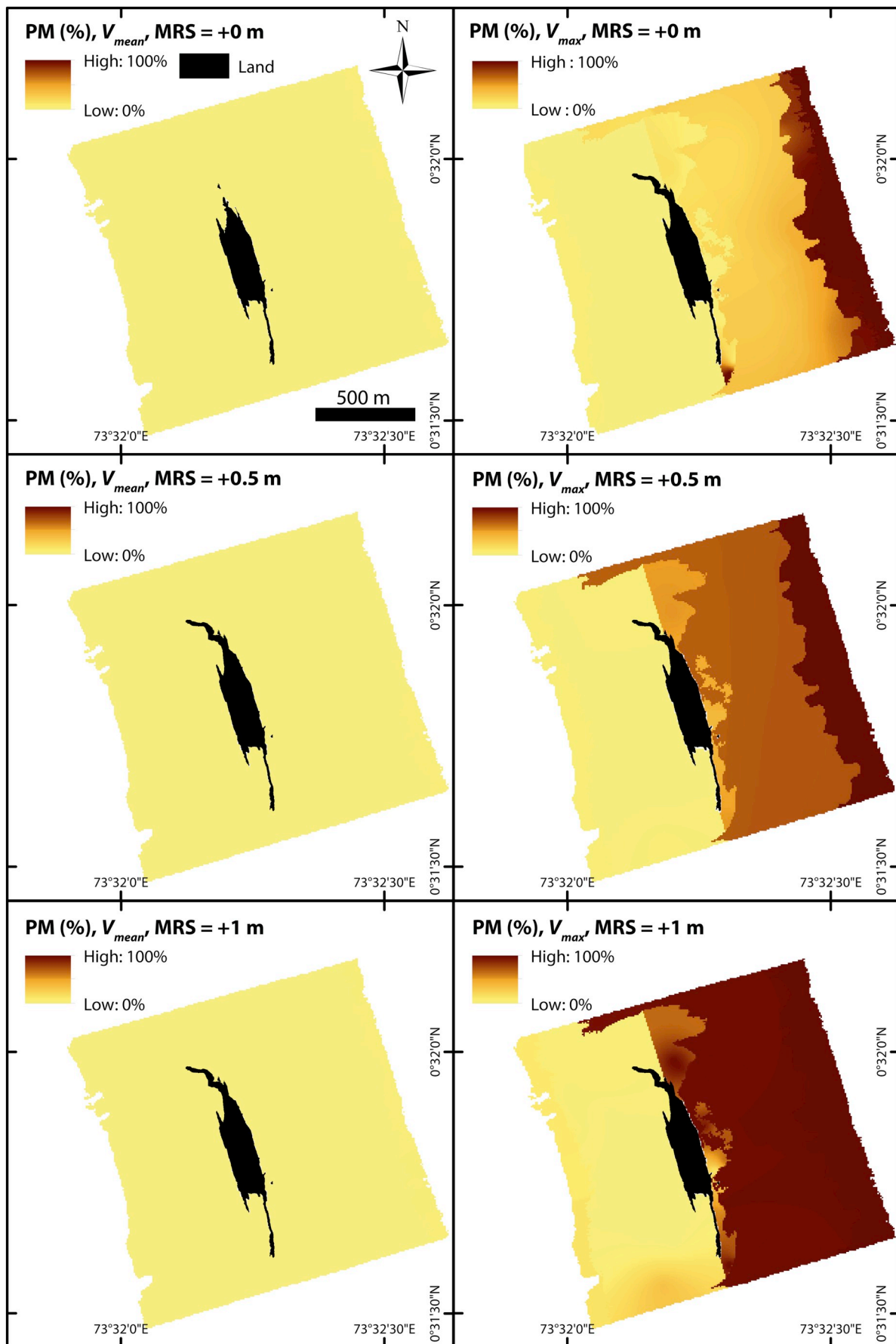


Fig. 4. Leeward site block kriging results of sediment potential mobility (PM, %) with both mean ( $V_{mean}$ ) and maximum ( $V_{max}$ ) velocities under scenarios of +0 m, +0.5 m, and +1 m MRS.

**Table 3**Potential Mobility (PM, %, mean  $\pm$  1 S.D., ranges in italics) of sediment within each eco-geomorphic zone where MRS = +0 m, +0.5 m and +1 m.

Site	Zone	MRS = +0 m		MRS = +0.5 m		MRS = +1 m		
		Mean $\pm$ 1 S.D.	Range	Mean $\pm$ 1 S.D.	Range	Mean $\pm$ 1 S.D.	Range	
Windward	$V_{mean}$ (PM, %)	ORC	20 $\pm$ 13.7	<i>2–51</i>	27.4 $\pm$ 14.6	<i>7–54</i>	37.9 $\pm$ 20.8	<i>8–80</i>
		R	10.3 $\pm$ 20.7	<i>0.5–84</i>	19.2 $\pm$ 20.8	<i>3–89</i>	20.4 $\pm$ 21.3	<i>5–93</i>
		OP	11 $\pm$ 23.7	<i>0–100</i>	16.2 $\pm$ 22.9	<i>0–100</i>	16.8 $\pm$ 23.2	<i>0–100</i>
		LS	1.5 $\pm$ 6	<i>0–24</i>	1.2 $\pm$ 4.5	<i>0–18</i>	0.8 $\pm$ 2.1	<i>0–7</i>
		LP	0.3 $\pm$ 0.7	<i>0–2</i>	0 $\pm$ 0	<i>0–0</i>	0 $\pm$ 0	<i>0–0</i>
		ORC	100 $\pm$ 0	<i>100–100</i>	100 $\pm$ 0	<i>100–100</i>	100 $\pm$ 0	<i>100–100</i>
	$V_{max}$ (PM, %)	R	99.9 $\pm$ 0.2	<i>99.5–100</i>	100 $\pm$ 0	<i>100–100</i>	100 $\pm$ 0	<i>100–100</i>
		OP	96.9 $\pm$ 12.6	<i>48–100</i>	100 $\pm$ 0	<i>100–100</i>	100 $\pm$ 0	<i>100–100</i>
		LS	8.3 $\pm$ 24.7	<i>0–99</i>	15 $\pm$ 29.5	<i>0–99.5</i>	22.7 $\pm$ 38.6	<i>0–100</i>
		LP	23.5 $\pm$ 30.2	<i>0–83</i>	22.4 $\pm$ 26.4	<i>0–60</i>	30.6 $\pm$ 33.8	<i>0–85</i>
		ORC	1.5 $\pm$ 1.3	<i>0–4</i>	1.8 $\pm$ 1.7	<i>0.5–5.5</i>	4.3 $\pm$ 4.5	<i>0.5–18</i>
		OSS	0 $\pm$ 0	<i>0–0</i>	0 $\pm$ 0	<i>0–0</i>	0 $\pm$ 0	<i>0–0</i>
Leeward	$V_{mean}$ (PM, %)	DSG	0 $\pm$ 0	<i>0–0</i>	0 $\pm$ 0	<i>0–0</i>	0 $\pm$ 0	<i>0–0</i>
		OS	0 $\pm$ 0	<i>0–0</i>	0 $\pm$ 0	<i>0–0</i>	0 $\pm$ 0	<i>0–0</i>
		LP	0 $\pm$ 0	<i>0–0</i>	0 $\pm$ 0	<i>0–0</i>	0 $\pm$ 0	<i>0–0</i>
		LRC	1.7 $\pm$ 4.2	<i>0–15</i>	1.7 $\pm$ 4.2	<i>0–15</i>	1.7 $\pm$ 4.2	<i>0–15</i>
		ORC	100 $\pm$ 0	<i>100–100</i>	100 $\pm$ 0	<i>100–100</i>	100 $\pm$ 0	<i>100–100</i>
		OSS	97.3 $\pm$ 8.2	<i>68–100</i>	100 $\pm$ 0	<i>100–100</i>	100 $\pm$ 0	<i>100–100</i>
	$V_{max}$ (PM, %)	DSG	38.3 $\pm$ 26.3	<i>4–95</i>	81.7 $\pm$ 20.0	<i>40–100</i>	95.3 $\pm$ 7.5	<i>76–100</i>
		OS	7.7 $\pm$ 7.8	<i>1.5–30</i>	44.9 $\pm$ 23.1	<i>0–83</i>	86.2 $\pm$ 12.2	<i>54–100</i>
		LP	0 $\pm$ 0	<i>0–0</i>	0.6 $\pm$ 1.5	<i>0–5</i>	5.3 $\pm$ 15.4	<i>0–60</i>
		LRC	2.8 $\pm$ 5.3	<i>0–15</i>	3.1 $\pm$ 6.2	<i>0–20</i>	3.8 $\pm$ 8.3	<i>0–30</i>

Note that marked spatial variability exists within each zone. At the windward site, LP = lagoonward patch, LS = lagoonward sand, OP = oceanward patch, R = rubble, and ORC = oceanward reef crest. At the leeward site, LRC = lagoonward reef crest, LP = lagoonward patch, OS = oceanward sand, DSG = dense seagrass, OSS = oceanward sparser seagrass, and ORC = oceanward reef crest.

windward site, the projected increase in PM was significant between MRS = +0.5 and +1 m ( $P = .012$ ), but not between MRS = +0 and +0.5 m ( $P = 0.232$ ; Wilcoxon signed ranks tests).

At the leeward site under  $V_{mean}$ , shifts in PM were projected to be marginal. Indeed, the magnitude of change in sediment PM under  $V_{mean}$  was significantly larger at the windward site than the leeward site ( $P \leq .0005$ ; Mann-Whitney  $U$  test). The only projected increase in sediment PM under increased MRS was in the oceanward reef crest zone (to  $1.8 \pm 1.7\%$  and  $4.3 \pm 4.5\%$  where MRS = +0.5 and +1 m respectively). No significant increase in PM was thus found between +0 and +0.5 m MRS at the leeward site under  $V_{mean}$  ( $P = .133$ , Wilcoxon signed ranks test). However, increases in PM were significant between +0.5 and +1 m MRS ( $P = .001$ , Wilcoxon signed ranks test). Under  $V_{max}$ , PM was modelled as 100% under +0.5 m and +1 m MRS in both the oceanward reef crest and sparser seagrass zones. While projected shifts in PM were marginal towards the oceanward platform margins, the largest increases in sediment PM were found in the remainder of the oceanward zones. For example, increases in PM in the oceanward sand zone were projected to be sufficiently high that they would shift the zone from one of preferential deposition (under  $V_{max}$  MRS = +0 m, PM =  $7.7 \pm 7.8\%$ ) to preferential sediment transport (under  $V_{max}$  MRS = +1 m, PM =  $86.2 \pm 12.2\%$ ). In contrast, modelled increases in average PM within the lagoonward zones under  $V_{max}$  were only marginal (up to 5.3%). Under  $V_{max}$ , highly significant increases were projected in PM between both increased MRS increments (+0 to +0.5 m and +0.5 to +1 m;  $P \leq .0005$  in both cases, Wilcoxon signed ranks tests). The magnitude of change in sediment PM was significantly greater under  $V_{max}$  than  $V_{mean}$  ( $P = .046$ ; Wilcoxon signed ranks tests). In contrast to under  $V_{mean}$ , the magnitude of change in sediment PM under  $V_{max}$  was significantly larger at the leeward site than the windward site ( $P \leq .0005$ ; Mann-Whitney  $U$  test).

## 5. Discussion

### 5.1. Wave processes

Contemporary wave processes were characterised by a cross-reef

oceanward-lagoonward attenuation of wave height and associated wave velocities. Under scenarios of increased reef submergence, changes in wave processes were non-linear and non-uniform, with the magnitude of change varying between zones and between increased MRS projections. These findings contrast with widely-held assumptions that wave energy will increase linearly with sea-level rise (Ferrario et al., 2014; Quataert et al., 2015). Rather, our results highlight the complex nature of atoll rim process regimes.

Results suggest that wave velocities will decrease or remain constant within the oceanward reef crest zones under increasing reef submergence. Decreased velocities may be driven by a decrease in dissipation during wave breaking, with higher submergence allowing a wider surf zone to develop across the outer reef flat; or because the atoll rim will still induce wave transformation and breaking. In contrast, under increased MRS, pronounced increases in velocities were projected across reef flats, driven by an increase in wave height and velocities able to propagate across the outer reef crest. Such increased velocities across reef flats are primarily attributed to a decrease in dissipation from wave breaking at the reef crest, whereby greater water depths enable a larger proportion of incident wave energy to propagate onto the reef flats. In addition, a slower decay in wave attenuation may be forced by depth-limited constraints. In some instances, larger waves may be able to cross the reef crest without breaking and greater energies then 'leak' onto the reef platform surface (Brander et al., 2004; Kench et al., 2009a). Indeed, between MRS = +0 m and +1 m, there was a 63% and 253% increase in average wave energy on the reef flat at the windward and leeward sites, respectively. Furthermore, higher submergence decreases hydrodynamic roughness relative to water depth which limits frictional dissipation across the reef flat (Storlazzi et al., 2011). Decreases in live coral cover can also cause reductions in surface rugosity, which may cause further reductions in the frictional dissipation of waves (Harris et al., 2018). Mean velocities, driven by spatial differences in wave setup, are predicted to decrease across the reef flat as wave dissipation at the reef crest is reduced. The net effect of increasing reef submergence is that sediment transport processes will increase across the reef flat because of higher wave orbital velocities, with mean flow a less important control on sediment transport during

modal wave conditions.

While depth-averaged currents are presented, they are not necessarily representative of the currents that interact with the bed in reef systems (i.e. the reef canopy causes a reduction in velocity; [Pomeroy et al., 2017](#)). [Cuttler et al. \(2018\)](#) and [Pomeroy et al. \(2018\)](#) have discussed the contributions of different forcing (wave-driven or mean current) to sediment transport in reef systems and highlight the importance of wave-driven processes for inducing reef sediment transport.

### 5.2. Sediment potential mobility

Under the contemporary process regime (MRS = +0 m), there was minimal potential for sediment mobility under mean velocity conditions. However, it is apparent that maximum wave-induced velocities are able to activate oceanward-lagoonward sediment transport at both sites, even under fair-weather conditions. This transportable material comprises sand-sized sediments (Figs. A15, A16), which are found within the upper horizons of the adjacent reef islands ([East et al., 2016, 2018](#)). Hence, our findings suggest that active sedimentary linkages exist between reef islands and their adjacent marine environments under fair-weather conditions.

While data suggest active reef-to-island connectivity, it is pertinent to note that the windward islands are underpinned by conglomerate platforms (~0.4 m above MSL on their oceanward shorelines ([East et al., 2018](#))). Although sediment PM was high across the outer reef at the windward site, the transfer of sediments to ocean-facing island shorelines may be ineffective under present conditions as sediments would need to bypass the conglomerate platform. However, this barrier to transport may change as sea levels rise because (1) the beach will become more connected to the process regime; and (2) shoreline materials may be mobilised more readily.

At the windward site, sediment PM was 100% across almost the entirety of the oceanward environment under  $V_{max}$ . Hence, under present conditions, this site represents a sediment-limited setting ([Kench and McLean, 2004](#)) whereby there is a highly efficient and continuous oceanward-lagoonward transfer of all available sediments. As such, the windward site oceanward reef flat zones are generally swept bare of island building sand-sized sediments ([East et al., 2016](#)). In contrast, under present conditions, the leeward site represents a transport-limited setting where wave energies are insufficient to enable the transfer of sediments from oceanward to lagoonward zones. Hence, the oceanward reef flat zones at the leeward site were characterised by the widespread accumulation of sand-sized sediments.

At the windward site, the one exception to the near-unanimously high PM values (~100%) across the oceanward environment was in the embayment area off the central transect where PM = 48%. Such lower PM values suggest that the embayment represents a depositional sink for medium-to-fine grained sand. This is consistent with shoreline geomorphology as this was the only portion of the oceanward island shoreline to be composed of sand-sized sediments, while the remainder of the oceanward island margins were comprised of reef rubble and coral boulders. Sediment PM analysis thus provides support for the process of embayment infilling, which has been identified as a key mechanism of shoreline accretion in other regions with similar island morphologies ([Kench et al., 2015](#)) and has been hypothesized to have occurred within the windward study site during island development ([East et al., 2018](#)).

The modelled spatial variability in sediment potential mobility contrasts with that found on faro type reef platforms in the Maldives (Vabbinfaru, North Malé Atoll). [Morgan and Kench \(2016\)](#) found the highest PM values were associated with lagoonal deposits, whereas coarser outer reef rim sediments had lower PM values. This contrasts the trends found in the present study, in which PM was highest toward the oceanward platform rim and lowest within the lagoonward zones. Such differences are a function of the higher wave velocities (as opposed to differences in sediment texture) found on the atoll rim

(maximum wave velocities on Vabbinfaru =  $0.29 \text{ m s}^{-1}$ ; [Morgan and Kench, 2016](#)). Indeed, the oceanward margins of atoll rim platforms are exposed to open ocean swell, whereas locally-generated wind-driven waves are incident around faro type platform margins. Hence, we highlight the diversity of atoll reef platform process regimes, even at intra-regional scales.

Under scenarios of increased MRS, the non-linearity and non-uniformity of the shifts in wave processes with increased MRS, were mirrored by changes in sediment PM whereby marked inter- and intra-site variability was found in the magnitude of change. Nonetheless, the predominant oceanward-lagoonward sediment transport pathways remained consistent between MRS scenarios. Under  $V_{max}$ , the increase in sediment PM at the leeward site was significantly larger than at the windward site. This is due to the highly exposed nature of the windward setting whereby PM was almost uniformly at 100% under contemporary conditions across the oceanward environment and, hence, there was minimal (or no) potential for further increases. That is, the windward site is already a sediment-limited setting. In contrast, under increased MRS, the leeward site was characterised by the transition from a transport-limited to a more sediment-limited setting. This between-site variability in shifts in sediment PM under MRS scenarios highlights that reef island responses to future environmental change are likely to be diverse over local scales. Notably, while PM remained relatively consistent under increased MRS at the oceanward platform margins, the largest increases in PM were found across the remainder of the oceanward zones. Such inner reef flat zones are those immediately adjacent to oceanward island shorelines, which has important implications for future island stability.

### 5.3. Geomorphic implications

A crucial consequence of the projected shifts in wave process regime under SLR, is the potential increase in energy delivered to reef island shorelines ([Ogston and Field, 2010](#); [Storlazzi et al., 2011](#); [Beetham et al., 2016](#)). Higher wave energies may increase rates of shoreline erosion with reworked sediment transferred back into the marine environment ([Storlazzi et al., 2011](#)). In addition, with projected increases in the PM of marine sediments, islands may be recipients of increased volumes of sediment, resulting in shoreline accretion. The increases in sediment mobility were of sand-sized material (Figs. A15, A16) and thus of an appropriate grade to contribute to island building. Notably, under all scenarios of reef submergence, the lagoonward areas remained as depositional sinks characterised by the limited capacity of hydrodynamics to entrain sediment. This continued capacity for the storage and accumulation of sand-sized sediment highlights the potential for rim reef islands to persist under increased reef submergence.

While the mobility of reef island sediments was not investigated directly, our results have clear implications for predicting reef island landform change. Reef islands will continually adjust with shifts in the process regime of the type our model outputs suggest ([Beetham and Kench, 2014](#)). Under both scenarios of increased MRS, benthic areas immediately adjacent to the oceanward shorelines of both islands shifted from areas of preferential sediment deposition (i.e. storage) to preferential transport. Hence, erosion will likely occur along these oceanward shorelines. Conversely, benthic areas immediately lagoonward of island shorelines remained areas of preferential deposition in both settings. This implies that sediment may be removed from oceanward areas and subsequently deposited in lagoonward areas. This deposited material may either remain below MSL as a benthic deposit or it may attain elevations above MSL, contributing to island accretion. Island accretion may occur via two key mechanisms: (1) 'roll-around' whereby alongshore sediment fluxes facilitate oceanward-lagoonward sediment transport and subsequent alongshore deposition; and/or (2) 'roll-over', or lateral migration, as material from the oceanward coast is eroded and deposited towards the lagoon ([Woodroffe et al., 1999](#)). Both processes of roll-around and roll-over could result in horizontal and

vertical lagoonward island accretion and thus net island migration. Hence, with a combination of oceanward shoreline erosion and lagoonward shoreline accretion, we hypothesize that increases in MRS may result in lagoonward island migration.

Our hypothesis that increased MRS may drive lagoonward island migration is consistent with several lines of evidence: (1) Analyses of island shoreline evolution over decadal timescales have found island lagoonward migration to occur under SLR. For example, following analyses of all 101 islands of Tuvalu, [Kench et al. \(2018\)](#) suggested there was compelling evidence that SLR was causing the lagoonward migration of atoll rim islands. Similarly, at Funafuti Atoll, which has experienced some of the highest rates of SLR ( $\sim 5.1 \pm 0.7 \text{ mm yr}^{-1}$ ), the predominant direction of island migration was lagoonwards ([Kench et al., 2015](#)). Furthermore, [Aslam and Kench \(2017\)](#) analysed shoreline island change on 184 islands in Huvadhu atoll and found lagoonward migration of rim islands to be the second most common mode of island change. Hence, whilst [Aslam and Kench \(2017\)](#) quantified island evolution, here we are able to examine the process mechanism that drives this mode of reef island change. (2) Analytical modelling of reef island futures under SLR and shifts in sediment supply found that island lagoonward migration occurred under all SLR scenarios ([Cowell and Kench, 2001](#); [Kench and Cowell, 2001](#)). (3) Palaeo-reconstructions of island evolution within the present study sites (based on 28 core records and 40 AMS radiocarbon dates) reveal notable parallels between the suggestions of future and former island roll-over and roll-around ([East et al., 2018](#)). Specifically, roll-over and roll-around were identified as key modes of reef island formation at these sites, likely controlled by higher than present sea levels associated with the mid-Holocene sea-level highstand ([Kench et al., 2009b](#)). Results of sediment PM analysis under increased MRS therefore support the suggestion that SLR could lead to a reactivation of the process regime responsible for reef island formation. In turn, future SLR could induce further island building and remobilisation.

Processes of island roll-around and roll-over would likely be most prevalent at the leeward site because the increase in sediment PM under increased MRS was significantly larger at the leeward site than at the windward site. Hence, leeward rim islands may become more mobile under scenarios of increased MRS than their windward counterparts. This suggestion is supported by prior work within the present study sites which has shown the leeward rim islands have been more mobile than windward rim islands over both millennial ([East et al., 2018](#)) and decadal ([Aslam and Kench, 2017](#)) timescales. In addition, numerical modelling of atoll reef island shorelines under SLR in the Pacific has suggested that lagoonward migration of leeward atoll islands may occur under scenarios of increased wave energy ([Shope et al., 2017](#)). We thus suggest that reef island future landform trajectories may be diverse and site-specific, even over local scales. The approach we present in this study provides a useful tool for investigating such trajectories of reef island systems.

Whilst the findings of this study imply that reef islands may persist into the future, albeit with increased island mobility, it is pertinent to note several caveats to this prognosis. Firstly, the present study investigates hydrodynamic processes and sediment transport under conditions associated with the upper confidence limits at the end of this century ([Perry et al., 2018](#)), however the upper limit of SLR projections by 2300 are substantially higher (up to 5.4 m under RCP8.5; [IPCC et al., 2019](#)). Secondly, the continued transport of sediment to reef island shorelines is largely contingent upon continued sediment production. Carbonate-producing organisms living in the adjacent reef environments represent the sole sediment source in atoll reef platform settings and thus any shift in reef ecology, and in the eco-geomorphic zones described in this study, will induce shifts in the rates and types of sediment production. Continued sediment production poses a particular challenge as coral reefs face a range of threats under climate change, including increases in ocean acidity and sea surface temperatures ([IPCC et al., 2019](#)). In the absence of continued sediment production, island

persistence would be contingent upon the storage and adjustment of a finite volume of sediment. Thirdly, whilst increased rates of island migration may enable the physical persistence of reef islands, such shifts in island planform will likely pose a challenge to the infrastructure and communities living in reef island nations. Fourthly, suggestions of future increases in island mobility assume that natural processes are able to occur. However, if human constructions (e.g. sea walls, jetties, harbour basins, breakwaters) hinder cross- and/or long-shore sediment transport ([Duvat et al., 2019](#)), the capacity of an island to adapt (e.g. through lagoonward island migration) to increased MRS will be compromised. We therefore highlight the importance of allowing natural sediment transport processes to occur in order to maximise the physical resilience of reef islands to sea-level rise.

## 6. Conclusion

We present the first projections of reef hydrodynamics and benthic sediment transport under MRS scenarios in an atoll reef island platform setting. Under the fair-weather contemporary process regime, this work indicates that benthic sediment transport is occurring on atoll rim platforms with active reef-to-island sediment connectivity. Under conditions of increased MRS, shifts in wave processes and sediment potential mobility were non-linear and non-uniform, counter to general assumptions that reef systems will respond linearly to environmental change. Specifically, under increased MRS, both wave velocities and sediment PM decreased or remained constant at the oceanward platform margins, whereas the largest increases were found on the inner reef flat. The lagoonal zones were projected to remain as sinks for sediment deposition under increased MRS. This continued capacity for sediment storage and deposition indicates that reef islands may persist under increased MRS. Due to the coupling of increased sediment PM adjacent to oceanward island shorelines and low sediment PM adjacent to lagoonward island shorelines, we hypothesize that lagoonward reef island migration will occur under increased MRS. Significant between-site differences were found in shifts in sediment PM under increased MRS, which implies that reef system, and in turn reef island, morphological responses to future increases in MRS are likely to be diverse and site-specific, even over local scales. As shifts in sediment PM were significantly larger in magnitude on the leeward rim than on the windward rim, we suggest that geomorphic shifts in reef island shorelines will be most pronounced on the leeward rim. These findings have implications for predicting the future adaptive capacity of atoll nations globally. Specifically, our results highlight the need for national-scale vulnerability assessments to incorporate (1) potential increases in island mobility; (2) the importance of allowing natural sediment transport processes to occur (unhindered by human constructions); and (3) intra-regional diversity in reef system geomorphic responses to sea-level rise.

## Declaration of Competing Interest

None

## Acknowledgements

This work was supported by a Natural Environment Research Council (NERC) PhD studentship (NE/K500902/1) and a DigitalGlobe Foundation imagery grant. We thank Mohamed Aslam and the Small Island Research Institute for facilitating fieldwork.

## Appendix A. Supplementary data

Supplementary data to this article can be found online at <https://doi.org/10.1016/j.gloplacha.2020.103196>.

## References

- Aslam, M., Kench, P.S., 2017. Reef island dynamics and mechanisms of change in Huvadhu Atoll, Republic of Maldives, Indian Ocean. *Anthropocene* 18, 57–68. <https://doi.org/10.1016/j.jancene.2017.05.003>.
- Beetham, E.P., Kench, P.S., 2014. Wave energy gradients and shoreline change on Vabbinfaru platform, Maldives. *Geomorphology* 209, 98–110. <https://doi.org/10.1016/j.geomorph.2013.11.029>.
- Beetham, E., Kench, P.S., O'Callaghan, J., Popinet, S., 2016. Wave transformation and shoreline water level on Funafuti Atoll, Tuvalu. *J. Geophys. Res. Oceans* 121, 311–326. <https://doi.org/10.1002/2015JC011246>.
- Beetham, E., Kench, P.S., Popinet, S., 2017. Future reef growth can mitigate physical impacts of sea-level rise on Atoll Islands. *Earth's Future* 5, 1002–1014. <https://doi.org/10.1002/2017EF000589>.
- Beetham, E., Kench, P.S., Popinet, S., 2018. Model skill and sensitivity for simulating wave processes on coral reefs using a shock-capturing Green-Naghdi solver. *J. Coast. Res.* <https://doi.org/10.2112/JCOASTRES-D-17-00117.1>.
- Bonneton, P., Chazel, F., Lannes, D., Marche, F., Tissier, M., 2011. A splitting approach for the fully nonlinear and weakly dispersive Green-Naghdi model. *J. Comput. Phys.* 230, 1479–1498. <https://doi.org/10.1016/j.jcp.2010.11.015>.
- Braithwaite, C.J.R., 1973. Settling behaviour related to sieve analysis of skeletal sands. *Sedimentology* 20, 251–262. <https://doi.org/10.1111/j.1365-3091.1973.tb02048.x>.
- Brander, R.W., Kench, P.S., Hart, D., 2004. Spatial and temporal variations in wave characteristics across a reef platform, Warraber Island, Torres Strait, Australia. *Mar. Geol.* 207, 169–184. <https://doi.org/10.1016/j.margeo.2004.03.014>.
- Chave, K.E., Smith, S.V., Roy, K.J., 1972. Carbonate production by coral reefs. *Mar. Geol.* 12, 123–140. [https://doi.org/10.1016/0025-3227\(72\)90024-2](https://doi.org/10.1016/0025-3227(72)90024-2).
- Congalton, R.G., 1991. A review of assessing the accuracy of classifications of remotely sensed data. *Remote Sens. Environ.* 37, 35–46. [https://doi.org/10.1016/0034-4257\(91\)90048-B](https://doi.org/10.1016/0034-4257(91)90048-B).
- Cowell, P.J., Kench, P.S., 2001. The morphological response of Atoll Islands to sea-level rise. Part 1: modifications to the shoreface translation model. *J. Coast. Res.* 633–644.
- Cuttler, M.V.W., Lowe, R.J., Falter, J.L., Buscombe, D., 2017. Estimating the settling velocity of bioclastic sediment using common grain-size analysis techniques. *Sedimentology* 64, 987–1004. <https://doi.org/10.1111/sed.12338>.
- Cuttler, M.V.W., Hansen, J.E., Lowe, R.J., Drost, E.J.F., 2018. Response of a fringing reef coastline to the direct impact of a tropical cyclone. *Limnol. Oceanogr. Lett.* 3 (2), 31–38. <https://doi.org/10.1002/loj2.10067>.
- Cuttler, M.V.W., Hansen, J.E., Lowe, R.J., Trotter, J.A., McCulloch, M.T., 2019. Source and supply of sediment to a shoreline salient in a fringing reef environment. *Earth Surf. Process. Landf.* 44, 552–564. <https://doi.org/10.1002/esp.4516>.
- Durrant, T., Hemer, M., Trenham, C., Greenslade, D., 2013. *CAWCR Wave Hindcast 1979–2010 (No. v5)*. CSIRO.
- Duvat, V.K.E., Magnan, A.K., 2019. Rapid human-driven undermining of atoll island capacity to adjust to ocean climate-related pressures. *Scientific Reports* 9 (15129). <https://doi.org/10.1038/s41598-019-51468-3>.
- Duvat, V.K.E., Salvat, B., Salmon, C., 2017. Drivers of shoreline change in atoll reef islands of the Tuamotu Archipelago, French Polynesia. *Glob. Planet. Chang.* 158, 134–154. <https://doi.org/10.1016/j.gloplacha.2017.09.016>.
- East, H.K., 2017. The evolution of Maldivian coral reef rim islands. In: *PhD Thesis*. University of Exeter, UK.
- East, H.K., Perry, C.T., Kench, P.S., Liang, Y., 2016. Atoll-scale comparisons of the sedimentary structure of coral reef rim islands, Huvadhu Atoll, Maldives. *J. Coast. Res.* 577–581. <https://doi.org/10.2112/SI75-116.1>.
- East, H.K., Perry, C.T., Kench, P.S., Liang, Y., Gulliver, P., 2018. Coral Reef Island Initiation and Development Under Higher Than Present Sea Levels. *Geophys. Res. Lett.* 45. <https://doi.org/10.1029/2018GL079589>.
- Ferrario, F., Beck, M.W., Storlazzi, C.D., Micheli, F., Shepard, C.C., Airolidi, L., 2014. The effectiveness of coral reefs for coastal hazard risk reduction and adaptation. *Nat. Commun.* 5, 3794. <https://doi.org/10.1038/ncomms4794>.
- Ford, M.R., Kench, P.S., 2012. The durability of bioclastic sediments and implications for coral reef deposit formation. *Sedimentology* 59, 830–842. <https://doi.org/10.1111/j.1365-3091.2011.01281.x>.
- Gibbs, R.J., Matthews, M.D., Link, D.A., 1971. The relationship between sphere size and settling velocity. *J. Sediment. Res.* 41, 7–18. <https://doi.org/10.1306/74D721D0-2B21-11D7-8648000102C1865D>.
- Grady, A.E., Moore, L.J., Storlazzi, C.D., Elias, E., Reidenbach, M.A., 2013. The influence of sea level rise and changes in fringing reef morphology on gradients in alongshore sediment transport. *Geophys. Res. Lett.* 40, 3096–3101. <https://doi.org/10.1002/grl.50577>.
- Hamylton, S.M., Hedley, J.D., Beaman, R.J., 2015. Derivation of high-resolution bathymetry from multispectral satellite imagery: a comparison of empirical and optimisation methods through geographical error analysis. *Remote Sens.* 7, 16257–16273. <https://doi.org/10.3390/rs71215829>.
- Harris, D.L., Rovere, A., Casella, E., Power, H., Canavesio, R., Collin, A., Pomeroy, A., Webster, J.M., Parravicini, V., 2018. Coral reef structural complexity provides important coastal protection from waves under rising sea levels. *Sci. Adv.* 4. <https://doi.org/10.1126/sciadv.aao4350>. eao4350.
- Hasselmann, K., Barnett, T.P., Bouws, E., Carlson, H., Cartwright, D.E., Enke, K., Ewing, J.A., Gienapp, H., Hasselmann, D.E., Kruseman, P., Meerburg, A., Müller, P., Olbers, D.J., Richter, K., Sell, W., Walden, H., 1973. Measurements of wind-wave growth and swell decay during the Joint North Sea Wave Project (JONSWAP). *Ergänzungsheft* 8–12.
- Hjulstrom, F., 1935. Studies of the morphological activity of rivers as illustrated by the River Fyris, *Bulletin. Geol. Inst. Upsala* 25, 221–527.
- IPCC, Oppenheimer, M., Glavovic, B., Hinkel, J., van de Wal, R.S.W., Magnan, A., Abd-Elgawad, A., Cai, R., Cifuentes-Jara, M., Conto, R., Ghosh, T., Hay, J., Isla, F., Marzeion, B., Meyssignac, B., Sebesvari, Z., 2019. Sea level rise and implications for low lying islands, coasts and communities. In: Pörtner, H.-O., Roberts, D.C., Masson-Delmotte, V., Zhai, P., Tignor, M., Poloczanska, E. ... Weyer, N. (Eds.), *IPCC Special Report on the Ocean and Cryosphere in a Changing Climate*, pp. 169.
- Kench, P.S., 1998. A currents of removal approach for interpreting carbonate sedimentary processes. *Mar. Geol.* 145, 197–223. [https://doi.org/10.1016/S0025-3227\(97\)00101-1](https://doi.org/10.1016/S0025-3227(97)00101-1).
- Kench, P.S., 2013. Coral systems (Volume Editor) In: Sherman, D.J. (Ed.), *Treatise on Geomorphology*. Academic Press, San Diego, pp. 328–359.
- Kench, P.S., Cowell, P.J., 2001. The morphological response of Atoll Islands to sea-level rise. Part 2: application of the modified shoreface translation model (STM). *J. Coast. Res.* 645–656.
- Kench, P.S., McLean, R.F., 1996. Hydraulic characteristics of bioclastic deposits: new possibilities for environmental interpretation using settling velocity fractions. *Sedimentology* 43, 561–570. <https://doi.org/10.1046/j.1365-3091.1996.d01-23.x>.
- Kench, P.S., McLean, R.F., 2004. Hydrodynamics and sediment flux of hwa in an Indian Ocean atoll. *Earth Surf. Process. Landf.* 29, 933–953. <https://doi.org/10.1002/esp.1072>.
- Kench, P.S., Brander, R.W., Parnell, K.E., McLean, R.F., 2006. Wave energy gradients across a Maldivian atoll: Implications for island geomorphology. *Geomorphology* 81, 1–17. <https://doi.org/10.1016/j.geomorph.2006.03.003>.
- Kench, P.S., Brander, R.W., Parnell, K.E., O'Callaghan, J.M., 2009a. Seasonal variations in wave characteristics around a coral reef island, South Maalhosmadulu atoll, Maldives. *Mar. Geol.* 262, 116–129. <https://doi.org/10.1016/j.margeo.2009.03.018>.
- Kench, P.S., Smithers, S.G., McLean, R.F., Nichol, S.L., 2009b. Holocene reef growth in the Maldives: evidence of a mid-Holocene sea-level highstand in the central Indian Ocean. *Geology* 37, 455–458. <https://doi.org/10.1130/G25590A.1>.
- Kench, P.S., Thompson, D., Ford, M.R., Ogawa, H., McLean, R.F., 2015. Coral islands defy sea-level rise over the past century: records from a central Pacific atoll. *Geology* 43, 515–518. <https://doi.org/10.1130/G36555.1>.
- Kench, P.S., Ford, M.R., Owen, S.D., 2018. Patterns of island change and persistence offer alternate adaptation pathways for atoll nations. *Nat. Commun.* 9, 605. <https://doi.org/10.1038/s41467-018-02954-1>.
- Lannes, D., Marche, F., 2015. A new class of fully nonlinear and weakly dispersive Green-Naghdi models for efficient 2D simulations. *J. Comput. Phys.* 282, 238–268. <https://doi.org/10.1016/j.jcp.2014.11.016>.
- Maiklem, W.R., 1968. Some Hydraulic properties of bioclastic carbonate grains. *Sedimentology* 10, 101–109. <https://doi.org/10.1111/j.1365-3091.1968.tb01102.x>.
- Mandler, P.G., 2008. *Wave processes in Huvadhu Atoll: Maldives, Indian Ocean (Masters of Science Thesis)*. University of Auckland.
- Morgan, K.M., Kench, P.S., 2014. A detrital sediment budget of a Maldivian reef platform. *Geomorphol. Coral Reef Geomorphol.* 222, 122–131. <https://doi.org/10.1016/j.geomorph.2014.02.013>.
- Morgan, K.M., Kench, P.S., 2016. Reef to island sediment connections on a Maldivian carbonate platform: using benthic ecology and biosedimentary depositional facies to examine island-building potential. *Earth Surf. Process. Landf.* 41, 1815–1825. <https://doi.org/10.1002/esp.3946>.
- Naseer, A., Hatcher, B.G., 2004. Inventory of the Maldives' coral reefs using morphometrics generated from Landsat ETM+ imagery. *Coral Reefs* 23, 161–168. <https://doi.org/10.1007/s00338-003-0366-6>.
- Ogston, A.S., Field, M.E., 2010. Predictions of turbidity due to enhanced sediment re-suspension resulting from sea-level rise on a fringing coral reef: evidence from Molokai, Hawaii. *J. Coast. Res.* 1027–1037. <https://doi.org/10.2112/JCOASTRES-D-09-00064.1>.
- Perry, C.T., Kench, P.S., O'Leary, M.J., Morgan, K.M., Januchowski-Hartley, F., 2015. Linking reef ecology to island building: Parrotfish identified as major producers of island-building sediment in the Maldives. *Geology* 43, 503–506. <https://doi.org/10.1130/G36623.1>.
- Perry, C.T., Alvarez-Filip, L., Graham, N.A.J., Mumby, P.J., Wilson, S.K., Kench, P.S., Manzello, D.P., Morgan, K.M., Slangen, A.B.A., Thomson, D.P., Januchowski-Hartley, F., Smithers, S.G., Steneck, R.S., Carlton, R., Edinger, E.N., Enochs, I.C., Estrada-Saldívar, N., Haywood, M.D.E., Kolodziej, G., Murphy, G.N., Pérez-Cervantes, E., Suchley, A., Valentino, L., Boenish, R., Wilson, M., Macdonald, C., 2018. Loss of coral reef growth capacity to track future increases in sea level. *Nature* 558, 396–400. <https://doi.org/10.1038/s41586-018-0194-z>.
- Pomeroy, A.W., Lowe, R.J., Ghisalberti, M., Storlazzi, C., Symonds, G., Roelvink, D., 2017. Sediment transport in the presence of large reef bottom roughness. *J. Geophys. Res. Oceans* 122 (2), 1347–1368. <https://doi.org/10.1002/2016JC011755>.
- Pomeroy, A.W.M., Lowe, R.J., Ghisalberti, M., Winter, G., Storlazzi, C., Cuttler, M., 2018. Spatial variability of sediment transport processes over intratidal and subtidal timescales within a fringing coral reef system. *J. Geophys. Res. Earth Surf.* 123, 1013–1034. <https://doi.org/10.1002/2017JF004468>.
- Popinet, S., 2015. A quadtree-adaptive multigrid solver for the Serre-Green-Naghdi equations. *J. Comput. Phys.* 302, 336–358. <https://doi.org/10.1016/j.jcp.2015.09.009>.
- Quataert, E., Storlazzi, C., van Rooijen, A., Cheriton, O., van Dongeren, A., 2015. The influence of coral reefs and climate change on wave-driven flooding of tropical coastlines. *Geophys. Res. Lett.* 42, 6407–6415. <https://doi.org/10.1002/2015GL064861>.
- Roeber, V., Cheung, K.F., 2012. Boussinesq-type model for energetic breaking waves in fringing reef environments. *Coast. Eng.* 70, 1–20. <https://doi.org/10.1016/j.coastaleng.2012.06.001>.
- Rouse, H., 1937. Modern conceptions of the mechanics of fluid turbulence. *Trans. Am. Soc. Civ. Eng.* 102, 463–505.

- Scoffin, T.P., 1987. *An Introduction to Carbonate Sediments and Rocks*. Blackwell, Glasgow.
- Scoffin, T.P., 1992. Taphonomy of coral reefs: a review. *Coral Reefs* 11, 57–77. <https://doi.org/10.1007/BF00357423>.
- Shields, A., 1936. Application of similarity principles and turbulence research to bed-load movement.
- Shope, J.B., Storlazzi, C., 2019. Assessing morphologic controls on atoll island alongshore sediment transport gradients due to future sea-level rise. *Front. Mar. Sci.* 6, 245. <https://doi.org/10.3389/fmars.2019.00245>.
- Shope, J.B., Storlazzi, C.D., Hoeke, R.K., 2017. Projected atoll shoreline and run-up changes in response to sea-level rise and varying large wave conditions at Wake and Midway Atolls, Northwestern Hawaiian Islands. *Geomorphology* 295, 537–550. <https://doi.org/10.1016/j.geomorph.2017.08.002>.
- Shore Protection Manual, 1984. *Shore Protection Manual*. Department of the Army, Waterways Experiment Station, Vicksburg, Mississippi.
- Sorby, H.C., 1879. The structure and origin of limestones. *Proc. Geol. Soc. Lond.* 35, 56–95.
- Storlazzi, C.D., Elias, E., Field, M.E., Presto, M.K., 2011. Numerical modeling of the impact of sea-level rise on fringing coral reef hydrodynamics and sediment transport. *Coral Reefs* 30, 83–96. <https://doi.org/10.1007/s00338-011-0723-9>.
- Storlazzi, C.D., Elias, E.P.L., Berkowitz, P., 2015. Many atolls may be uninhabitable within decades due to climate change. *Sci. Rep.* 5, 14546. <https://doi.org/10.1038/srep14546>.
- Storlazzi, C.D., Gingerich, S.B., van Dongeren, A., Cheriton, O.M., Swarzenski, P.W., Quataert, E., Voss, C.I., Field, D.W., Annamalai, H., Piniak, G.A., McCall, R., 2018. Most atolls will be uninhabitable by the mid-21st century because of sea-level rise exacerbating wave-driven flooding. *Sci. Adv.* 4 <https://doi.org/10.1126/sciadv.aap9741>. eap9741.
- Stumpf, R.P., Holderied, K., Sinclair, M., 2003. Determination of water depth with high-resolution satellite imagery over variable bottom types. *Limnol. Oceanogr.* 48, 547–556.
- SwellBeat, 2020. <https://swellbeat.com/wavecalculator/>.
- Tissier, M., Bonneton, P., Marche, F., Chazel, F., Lannes, D., 2012. A new approach to handle wave breaking in fully non-linear Boussinesq models. *Coast. Eng.* 67, 54–66. <https://doi.org/10.1016/j.coastaleng.2012.04.004>.
- Tolman, H.L., 2009. *User Manual and System Documentation of WAVEWATCH III TM Version 3.14*. (Technical note, MMAB Contribution No. v. 276).
- Webb, A.P., Kench, P.S., 2010. The dynamic response of reef islands to sea-level rise: Evidence from multi-decadal analysis of island change in the Central Pacific. *Glob. Planet. Chang.* 72, 234–246. <https://doi.org/10.1016/j.gloplacha.2010.05.003>.
- Woodroffe, C.D., 1993. Morphology and evolution of reef islands in the Maldives. In: *Proceedings of the 7th International Coral Reef Symposium 2*, pp. 1217–1226.
- Woodroffe, C.D., McLean, R.F., Smithers, S.G., Lawson, E.M., 1999. Atoll reef-island formation and response to sea-level change: West Island, Cocos (Keeling) Islands. *Mar. Geol.* 160, 85–104. [https://doi.org/10.1016/S0025-3227\(99\)00009-2](https://doi.org/10.1016/S0025-3227(99)00009-2).
- Wunderground, 2015. *Weather Underground*. [wunderground.com](http://wunderground.com).
- Young, I.R., 1999. Seasonal variability of the global ocean wind and wave climate. *Int. J. Climatol.* 19, 931–950. [https://doi.org/10.1002/\(SICI\)1097-0088\(199907\)19:9<931::AID-JOC412>3.0.CO;2-O](https://doi.org/10.1002/(SICI)1097-0088(199907)19:9<931::AID-JOC412>3.0.CO;2-O).